PNAS RESEARCH ARTICLE | CELL BIOLOGY

Lysis of human erythrocytes due to Piezo1-dependent cytosolic calcium overload as a mechanism of circulatory removal

Lennart Kuck[a,1], Antony P. McNamee[a], Maria Bordukova[b,c,d], Ario Sadafi[e,f], Carsten Marr[e], Jason N. Peart[g], and Michael J. Simmonds[a]

Affiliations are included on p. 10.

Edited by Osama Harraz, University of Vermont, Burlington, Vermont; received April 23, 2024; accepted July 16, 2024 by Editorial Board Member Mark T. Nelson

Hematopoietic stem cells surrender organelles during differentiation, leaving mature red blood cells (RBC) devoid of transcriptional machinery and mitochondria. The resultant absence of cellular repair capacity limits RBC circulatory longevity, and old cells are removed from circulation. The specific age-dependent alterations required for this apparently targeted removal of RBC, however, remain elusive. Here, we assessed the function of Piezo1, a stretch-activated transmembrane cation channel, within subpopulations of RBC isolated based on physical properties associated with aging. We subsequently investigated the potential role of Piezo1 in RBC removal, using pharmacological and mechanobiological approaches. Dense (old) RBC were separated from whole blood using differential density centrifugation. Tolerance of RBC to mechanical forces within the physiological range was assessed on single-cell and cell population levels. Expression and function of Piezo1 were investigated in separated RBC populations by monitoring accumulation of cytosolic Ca^{2+} and changes in cell morphology in response to pharmacological Piezo1 stimulation and in response to physical forces. Despite decreased Piezo1 activity with increasing cell age, tolerance to prolonged Piezo1 stimulation declined sharply in older RBC, precipitating lysis. Cell lysis was immediately preceded by an acute reversal of density. We propose a Piezo1-dependent mechanism by which RBC may be removed from circulation: Upon adherence of these RBC to other tissues, they are uniquely exposed to prolonged mechanical forces. The resultant sustained activation of Piezo1 leads to a net influx of Ca^{2+}, overpowering the Ca^{2+}-removal capacity of specifically old RBC, which leads to reversal of ion gradients, dysregulated cell hydration, and ultimately osmotic lysis.

red blood cells | mechanotransduction | Piezo1 | calcium signaling | hemolysis

Significance

Mature red blood cells (RBC) are enucleated, devoid of cell organelles, and incapable of translational activity. Yet, the RBC lifespan is remarkably consistent, and the molecular underpinnings of this apparently timely and targeted removal of old RBC remain elusive. Here, we provide evidence to support a hypothesis for this removal process: Old RBC undergo lysis during prolonged exposure to mechanical force due to excessive influx of calcium ions *via* mechanosensitive channels. This pathway is consistent with clinical phenotypes of mutations in the *PIEZO1* gene, and the molecular players involved in this signaling cascade may present targets for pharmaceutical developments aimed at conditions associated with premature RBC clearance.

Red blood cells (RBC), the oxygen carriers in mammalian blood, continuously traverse the cardiovascular system for around 120 d (1, 2). During these ~120 d of vascular transit, RBC undergo a progressive decline of metabolic function, culminating in removal by macrophages (3–5). Impaired metabolism is of specific relevance in RBC, given that precursor cells eject their nucleus, mitochondria, and other organelles, leaving mature erythrocytes exclusively reliant on glycolytic ATP generation (6). As a result, RBC exhibit progressively decreased resting cytosolic ATP concentration and capacity for metabolic flux with increasing age (7–10). Given the large difference in calcium-ion concentration $[Ca^{2+}]$ between the RBC cytosol (30 to 90 nmol L^{-1}) and the suspending plasma [>1.5 mmol L^{-1}; (11)], opening of cation channels results in acute and significant increases of intracellular $[Ca^{2+}]$ [i.e., $(Ca^{2+})_i$]. Removal of cytosolic Ca^{2+} against this substantial concentration gradient occurs exclusively through plasma membrane calcium ATPases (PMCA) and requires ATP hydrolysis. Outward transport of Ca^{2+} is thus a profound threat to cellular homeostasis, particularly for older cells, which exhibit diminished PMCA activity (10) due to impaired metabolic capacity and decreased basal ATP availability (12–14).

Aging of RBC is also associated with a progressive increase in density, which allows for separation of RBC subpopulations according to their density (15). This densification is primarily attributed to the Gárdos effect, driven by an accumulation of $[Ca^{2+}]_i$ due to recurrent transient increases of $[Ca^{2+}]_i$ during each capillary transit (16–18). Increases in $[Ca^{2+}]_i$ activate the calcium-activated potassium channel $K_{Ca}3.1$ (i.e., the "Gárdos channel), which is sensitive to mild increases in $[Ca^{2+}]_i$ [~0.1 µmol L^{-1} activation threshold; (10, 19)]. Activation of the Gárdos channel results in K^+-efflux that drives loss of intracellular water due to local osmotic gradients, resulting in decreased cell volume (20).

Recent advances support that the Gárdos effect may be triggered acutely by transient mechanical cues following activation of mechanically gated ion channels (21, 22). Circulating RBC express the bona fide mechanosensory protein Piezo1, which has been implicated in regulation of RBC volume and nitric oxide metabolism by initiating Ca^{2+}

Competing interest statement: MB is employed by Roche Diagnostics GmbH but contributed to this research independently of her work at Roche Diagnostics GmbH as a guest scientist at Helmholtz Munich (Helmholtz Zentrum Muenchen–Deutsches Forschungszentrum fuer Gesundheit und Umwelt GmbH).

This article is a PNAS Direct Submission. O.F.H. is a guest editor invited by the Editorial Board.

[1]To whom correspondence may be addressed. Email: lennartkuck@gmail.com.

This article contains supporting information online at https://www.pnas.org/lookup/suppl/doi:10.1073/pnas.2407765121/-/DCSupplemental.

Published August 29, 2024.

signaling (21–23). Gain-of-function mutations in the gene encoding Piezo1 have been increasingly associated with anemias characterized by accelerated clearance of RBC, indicating that Piezo1 may play a role in regulating the targeted and timely removal of RBC from circulation (24, 25). While recent computational studies provide compelling evidence to support that Piezo1 is involved in regulating circulatory longevity of RBC (16), and indeed drives their aging patterns [e.g., promotes densification (26)], experimental evidence has not yet been provided. The aim of the present study was thus to examine the tolerance of subpopulations of RBC isolated based on their density to Ca^{2+} loading, assess the expression and function of Piezo1 in these subpopulations, and investigate the sensitivity of these cells to sustained mechanical stress and Piezo1 activation.

Results

Density-Separated Subpopulations of RBC Exhibit Distinct Cellular Properties. Hematological data of the three RBC subpopulations (i.e., young, middle, and old cells) obtained from healthy donors and the respective unfractionated control RBC populations are presented in Fig. 1. The most dense RBC fraction (i.e., old cells) had significantly lower mean cell volume (MCV) when compared with the other fractions (all $P < 0.05$; Fig. 1*B*). No differences in red cell distribution width (RDW) or red cell distribution width SD (RDW-SD) were observed (Fig. 1 *C* and *D*). HbA_{1c} was significantly increased in the old fraction of RBC when compared with the young fraction ($P < 0.05$; Fig. 1*E*). Further, cell deformability, expressed as elongation index assessed at specific fluid forces (i.e., shear stresses) of old RBC was significantly lower than that of unfractionated, young, and middle RBC over a broad range of physiologically relevant shear stresses (0.94 to 9.09 Pa; $P < 0.05$; Fig. 1*F*).

Old RBC are Sensitive to Calcium-Dependent Lysis During Prolonged Mechanical Stimulation. Changes in RBC subpopulation properties prior to and following prolonged mechanical stimulation at 10 Pa for 300 s in the absence, or presence, of plasma-equivalent calcium content (2 mmol L^{-1} $CaCl_2$) are presented in Fig. 2. Basal deformability of old RBC was lowest when compared with young and middle fractions

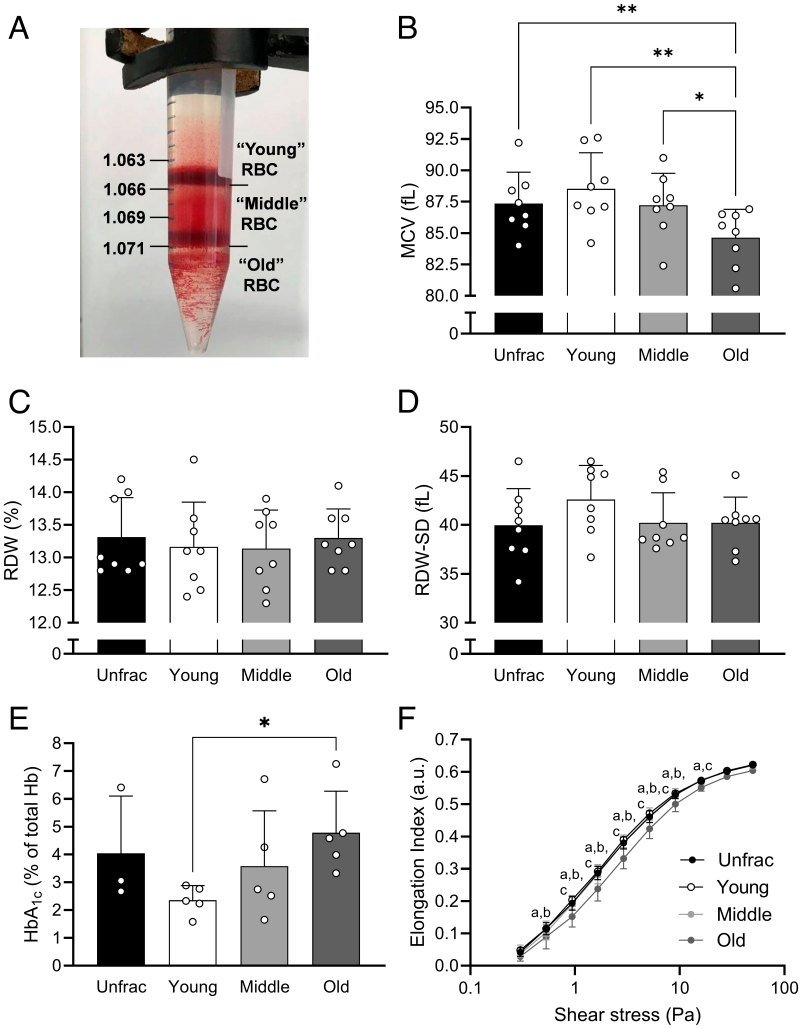

Fig. 1. Characterization of hematological, physical, and biochemical parameters of three red blood cell (RBC) subpopulations separated based on distinct densities. A representative result of the density fractionation process demonstrates the two distinct bands that were typically visible when separating RBC (*A*). RBC with densities of 1.066 g mL^{-1} and lower were extracted and labeled as the "young" cell fraction, RBC with densities between 1.066 and 1.069 g mL^{-1} as the "middle" fraction, and RBC with densities greater than 1.071 g mL^{-1} were considered "old" cells. Hematological characteristics of RBC subpopulations (i.e., unfractionated, "Unfrac"; Young; Middle, and; Old) were assessed using an automated analyzer (*B–D*); $n = 8$ blood samples obtained from distinct donors. The concentration of glycated hemoglobin relative to total hemoglobin was measured using a sandwich ELISA (*E*).; $n = 3$ to 5 blood samples. *P* values were calculated using one-way ANOVA with Dunnett's multiple comparisons test. Cellular deformability was measured under fluid shear stresses between 0.3 to 50.0 Pa using an ektacytometer (*F*); $n = 8$ blood samples. *P* values were calculated using two-way ANOVA. $^{**}P < 0.01$ and $^{*}P < 0.05$ between designated pairs. [a]Significant differences between unfractionated and old RBC; [b]significant differences between young and old RBC; [c]significant differences between middle and old RBC.

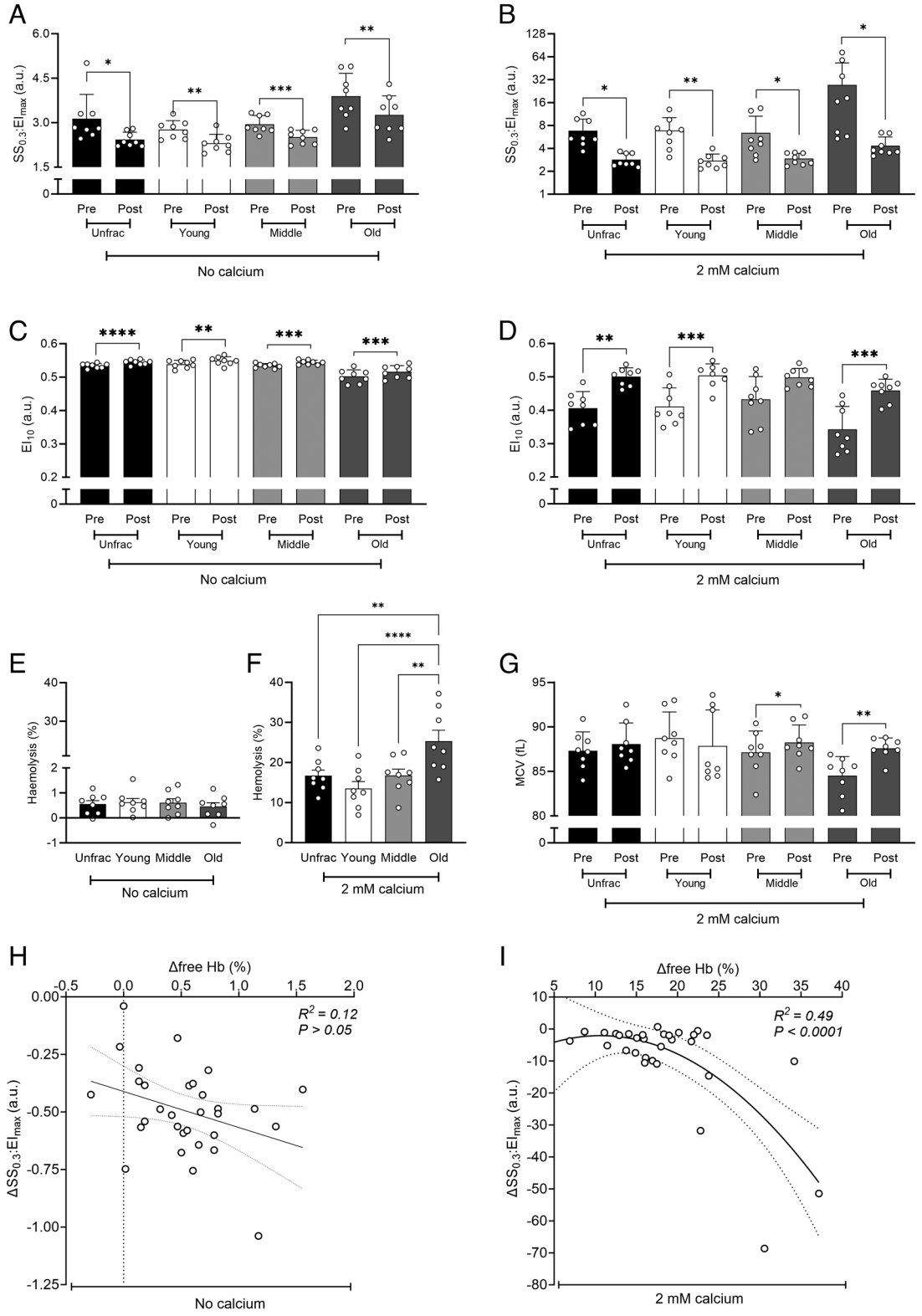

Fig. 2. Prolonged mechanical force application of 10 Pa for 300 s induces red blood cell (RBC) lysis, especially of old cells, in a calcium-dependent manner. All parameters were measured prior to ("Pre") and immediately following ("Post") mechanical stimulation. Stimulation was carried out in an identical manner using isotonic shearing media (*left column*) or shearing media supplemented with 2 mmol L^{-1} calcium chloride (*right column*, unless noted otherwise). Changes in RBC deformability are presented as an integrated index ($SS_{0.3}$:EI_{max}; *A* and *B*) and as elongation measured under 10 Pa of fluid shear stress (EI_{10}; *C* and *D*). Destruction of RBC as a result of mechanical stimulation was defined as release of hemoglobin into the shearing medium (i.e., hemolysis; *E* and *F*), while changes in cell volume are shown for RBC subpopulations sheared in the presence of calcium chloride (*G*). Correlation analyses relate the extent of hemolysis with change in $SS_{0.3}$:EI_{max} for individual "Pre" and "Post" blood samples (*H* and *I*). *P* values of Pre–Post comparisons were calculated using paired *t* tests. *P* values in *E* and *F* were calculated using one-way ANOVA with Bonferroni's post hoc test. $^{****}P < 0.0001$, $^{***}P < 0.001$, $^{**}P < 0.01$, and $^{*}P < 0.05$ between designated pairs. Data presented as means ± SD; *n* = 8 blood samples obtained from distinct donors.

(i.e., reflected by high values of $SS_{0.3}$:EI_{max}, A,B; lowest values of EI, C,D). Cellular deformability of all RBC subpopulations significantly increased ($P < 0.05$; Fig. 2 *A–D* and *SI Appendix*, Fig. S2) following mechanical stimulation ("Post"), relative to unstimulated baseline values ("Pre"). This improvement was most pronounced in the old cell subpopulation, particularly in the presence of 2 mmol L^{-1} $CaCl_2$ (Fig. 2 *B*, *D* and *G*). Further, substantial improvements in cellular deformability following mechanical stimulation were accompanied by significantly greater lysis of the old RBC subpopulation, when compared with those of unfractionated, young, or middle RBC populations (Fig. 2*F*), which occurred in concert with significantly increased MCV (Fig. 2*G*). Mechanical stimulation in the absence of extracellular $CaCl_2$, however, precipitated no difference in hemolysis (Fig. 2*E*).

Accordingly, there was no significant association between hemolysis levels following mechanical stimulation without $CaCl_2$ and corresponding improvements in RBC deformability (i.e., reflected by decreases in $SS_{0.3}$:EI_{max}; $R^2 = 0.12$, $P > 0.05$; Fig. 2*H*). When stimulated in the presence of 2 mmol L^{-1} $CaCl_2$, however, hemolysis was strongly and significantly associated with corresponding changes in $SS_{0.3}$:EI_{max} ($R^2 = 0.49$, $P < 0.0001$; Fig. 2*I*).

Given the improvements in cell population properties coinciding with lysis of some RBC, we hypothesized that those cells closest to the end of their lifespan (i.e., those with the most unfavorable mechanical properties) were most sensitive to prolonged mechanical stimulation in the presence of extracellular Ca^{2+}. Piezo1, a widely expressed stretch-activated cation channel that is also present in the RBC membrane (22), appears to be the primary transducer of mechanically activated signaling in this cell type (27, 28). Thus, we aimed to test whether old RBC were less capable of sustaining Piezo1-induced increases in $[Ca^{2+}]_i$.

Calcium-Handling Capacity is Impaired in Old RBC Despite Decreased Piezo1 Abundance. The basal fluorescent intensity of the Ca^{2+}-sensitive fluorescent probe Fluo-4 was highest in RBC obtained from the middle fraction, while old RBC exhibited the lowest intensity ($P < 0.01$; Fig. 3*A*). Following stimulation of RBC with 15 μmol L^{-1} Yoda1 (*SI Appendix*, Fig. S3), RBC presented with dramatically increased fluorescent intensity, irrespective of cell age. Sustained exposure to Yoda1 resulted in pronounced increases of fluorescent intensity in young RBC, when compared with old ($P < 0.01$; Fig. 3*B*). Young and middle RBC exhibited a decrease in fluorescent intensity following the initial increase in Fluo-4 fluorescence caused by acute Yoda1 exposure, while Fluo-4 fluorescence in old RBC failed to decrease during this period (Fig. 3*C*). Piezo1 abundance was then examined using in old and middle RBC relative to that of the youngest RBC using immunofluorescence with Piezo1-specific primary antibodies (*SI Appendix*, Fig. S4). Relative abundance of Piezo1 significantly decreased in old RBC when compared with younger cells ($P < 0.05$; Fig. 3*D*). Given that pharmacological opening of Piezo1 channels may mechanistically differ from opening induced by mechanical forces, we next aimed to examine whether stretch-induced changes in $[Ca^{2+}]_i$ of individual cells were different between the RBC subpopulations.

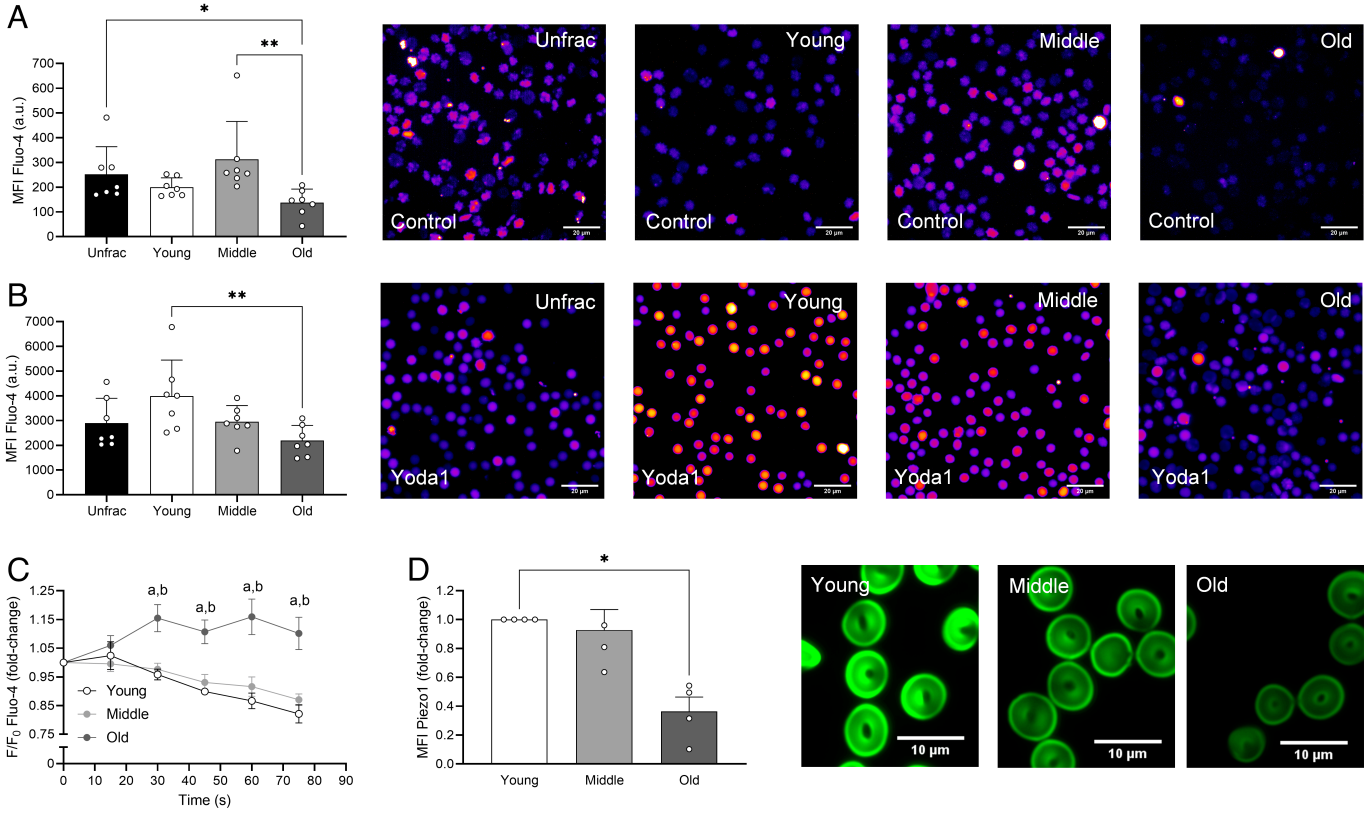

Fig. 3. Red blood cell (RBC) subpopulations of different in vivo ages exhibit altered calcium-handling capacity. Fluo-4 fluorescent intensity was measured in resting RBC following gradient-density separation (*A*; *P* values were calculated using Friedman's test with Dunn's multiple comparisons), and after 10 min of incubation with the Piezo1-specific activator Yoda1 (*B*; *P* values were calculated using one-way ANOVA with Bonferroni's post hoc test), $n = 7$ blood samples obtained from distinct donors. Dynamic changes in the fluorescent intensity of RBC subpopulations were tracked immediately following stimulation with Yoda1 (15 μmol L^{-1}; *C*), $n = 6$ blood samples. *P* values were calculated using two-way ANOVA. Changes in abundance of Piezo1 visualized by immunofluorescent staining are expressed relative to young cells, which reflect the maximal relative abundance (*D*; *P* values were calculated using Friedman's test with Dunn's multiple comparisons), $n = 4$ blood samples. [a]Significant differences between young and old; [b]significant differences between middle and old. $^{**}P < 0.01$ and $^{*}P < 0.05$.

Calcium Influx Through Mechanically Activated Ion Channels is Decreased in Old RBC. Micropipette aspiration was employed to assess calcium flux during entry into a narrow aperture (2 μm), which forces deformation of the cell membrane (Fig. 4*A*). Individual RBC of the distinct subpopulations loaded with Fluo-4 were aspirated into the pipette at a constant pressure of −5 mmHg (Fig. 4 *B* and *C*). During pilot testing, it was confirmed that aspiration of RBC at this pressure in a buffer without added Ca^{2+} did not cause cellular abnormalities or cell lysis to confirm that observed changes were not related to purely mechanically induced cell damage (*SI Appendix*, Fig. S5). Increases in Fluo-4 fluorescence during deformation were significantly greater in young (~1.8-fold, $P < 0.0001$; Fig. 4*D*) and middle RBC (~1.4-fold, $P < 0.01$; Fig. 4*D*) when compared with old RBC (~1.1-fold). Inhibition of mechanically sensitive channels through treatment of young RBC with 3.3 μM GsMTx4 completely abrogated the increase in fluorescence during aspiration ($P < 0.0001$; Fig. 4*D* and Movie S3). Of note, GsMTx4-treated cells were rigid and thus exhibited significantly shorter tongue length when aspirated into the pipette (Fig. 4 *C* and *E*).

Next, we aimed to assess whether the distinct Piezo1 sensitivity and Ca^{2+}-handling capacity of the isolated RBC subpopulations also translated to distinct morphological responses to Piezo1-dependent Ca^{2+} influx. Given that these effects are not visible during micropipette aspiration, we employed the Piezo1-specific activator Yoda1 in a static model.

Sustained Piezo1 Stimulation Causes Systematic Alterations in Cell Morphology. Treatment of RBC with 15 μmol L^{-1} of the Piezo1 activator Yoda1 caused significant changes in cell morphology irrespective of RBC age (Fig. 5). Cells exhibited significantly increased sphericity (Fig. 5*C*; all $P < 0.0001$), decreased area (Fig. 5*D*; all $P < 0.0001$), and increased solidity (Fig. 5*E*; all $P < 0.0001$) following Yoda1 exposure. Changes in these morphological parameters were most pronounced at 2 min of treatment, and further exacerbated at 5 min, although differences between 5 and 10 min appeared mild. Further, while overall changes in morphological features of RBC obtained from the different subpopulations appeared to follow a similar trend, we observed differences in kinetics between them. For example,

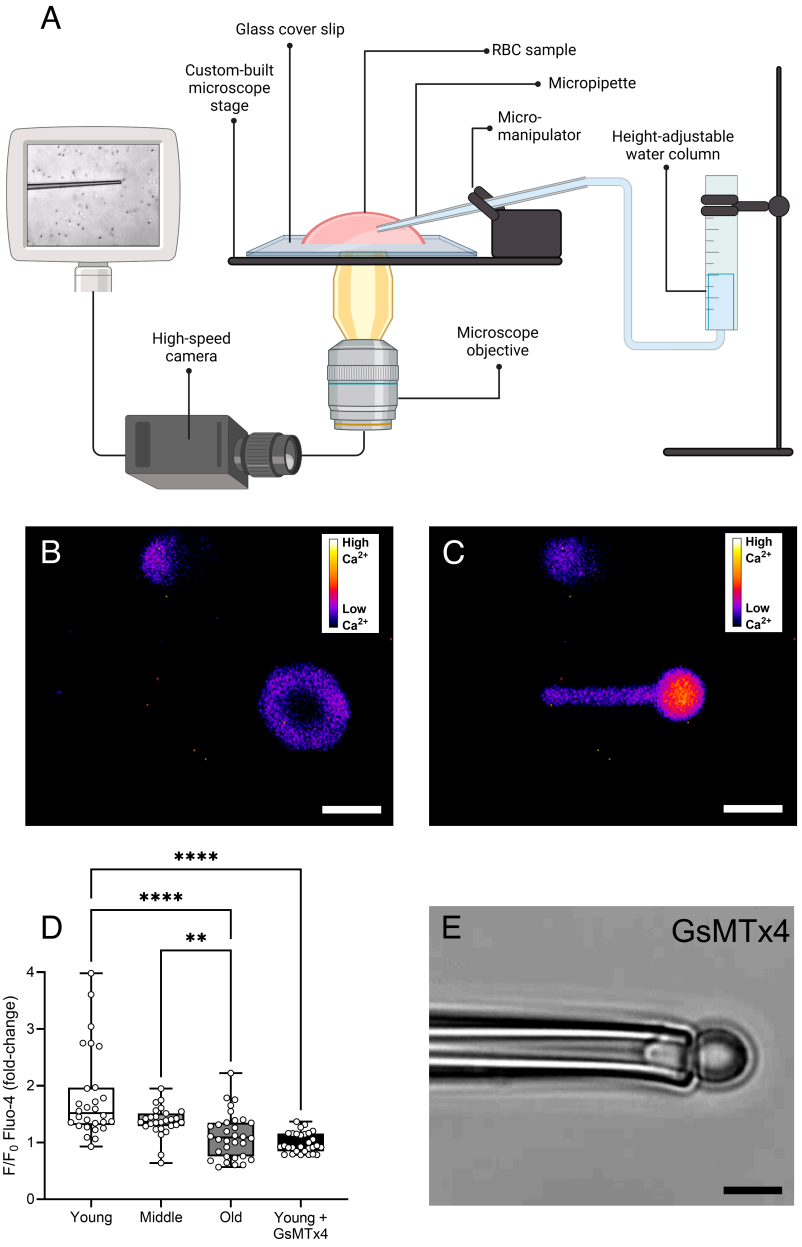

Fig. 4. Calcium flux into individual red blood cells (RBC) obtained from density-separated subpopulations during aspiration into a micropipette. A custom-developed micropipette aspiration apparatus was used to visualize mechanics and dynamic changes in calcium content of individual RBC undergoing deformation during aspiration into the 2-μm pipette tip (*A*). The fluorescent intensity of RBC loaded with the fluorescent calcium indicator Fluo-4 was measured at baseline (*B*) and during full aspiration into the micropipette operated at a suction pressure of −5 mmHg (*C*). The relative increase in fluorescence during aspiration over baseline levels was calculated for RBC of the different subpopulations, while young RBC treated with the mechanically sensitive channel inhibitor GsMTx4 served as negative control (*D*). *P* values were calculated using the Kruskal–Wallis test with Dunn's multiple comparisons. GsMTx4-treated cells exhibited substantially increased membrane rigidity and were thus not aspirated fully into the pipette at the pressure of −5 mmHg (*E*). $n = 27$ to 32 individual RBC from at least two distinct blood donors. (Scale bars, 5 μm.) $^{****}P < 0.0001$ and $^{**}P < 0.01$.

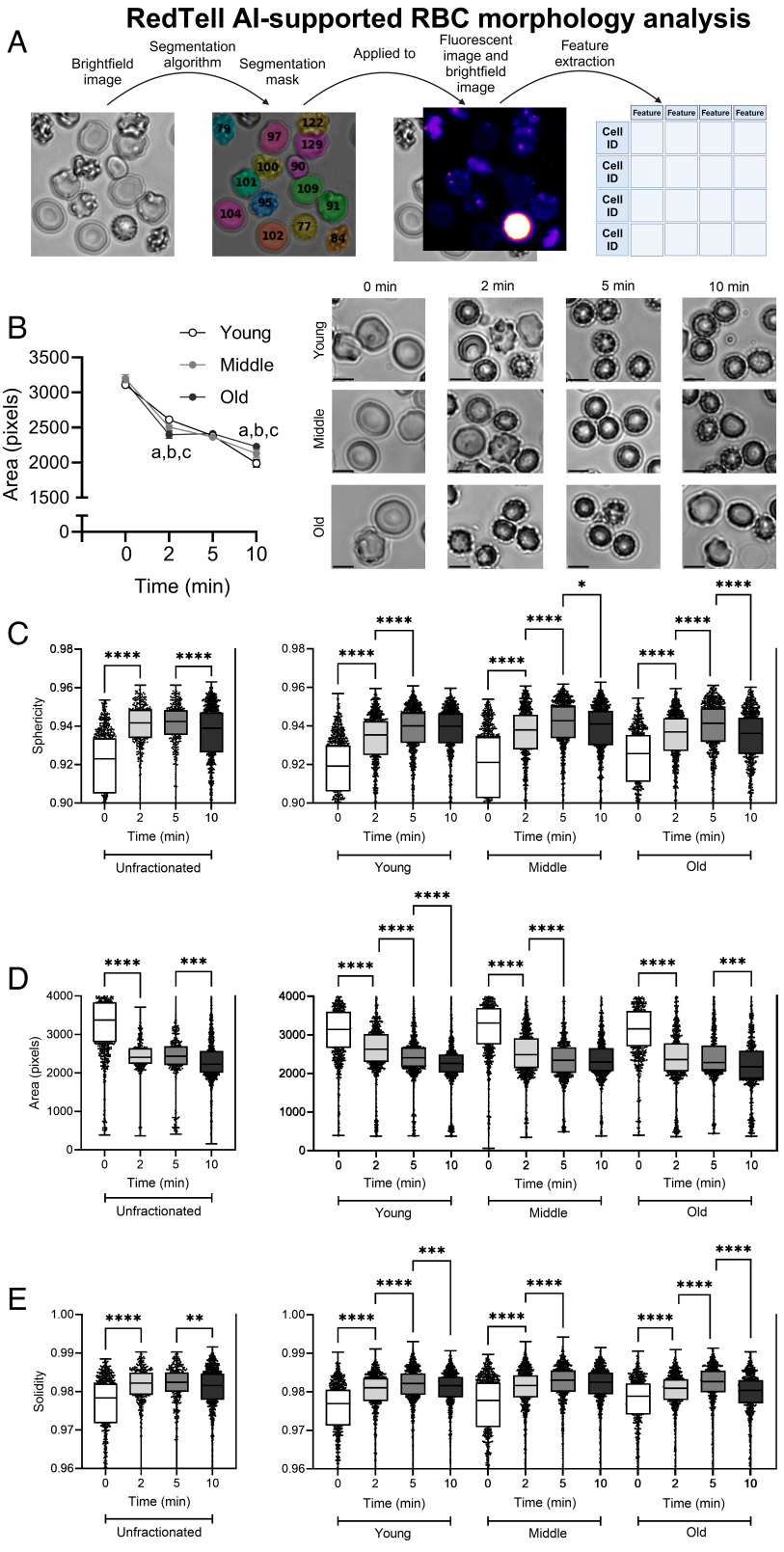

Fig. 5. Pharmacological activation of Piezo1 through Yoda1 exposure causes time-dependent alterations in red blood cell (RBC) morphology. Young, middle, and old RBC were exposed to 15 μmol L^{-1} Yoda1 over a period of 600 s. Images were then segmented using RedTell's artificial neural network, and features were extracted from individual RBC (*A*). Changes in features during Yoda1 treatment were extracted from images taken at baseline (0) and following 2, 5, and 10 min of exposure to Yoda1 (*B*; *P* values were calculated using two-way ANOVA). Biologically relevant morphological features including sphericity, cell area, and solidity were tracked in unfractionated RBC (Unfrac), and subpopulations of Young, Middle, and Old RBC (*C*–*E*). *P* values were calculated using Kruskal–Wallis tests with Dunn's multiple comparisons. [a]Significant differences between young and middle; [b]significant differences between young and old; [c]significant differences between middle and old. $^{****}P < 0.0001$, $^{**}P < 0.01$, and $^{*}P < 0.05$. n = 772 to 994 individual RBC from at least two distinct blood donors. (Scale bar, 5 μm.)

changes in the cell area of young RBC with 10 min of Yoda1 treatment followed a near-linear pattern, while changes in cell area of old RBC were significantly more pronounced during the first 2 min of exposure (Fig. 5*B*; $P < 0.0001$), followed by only a minor exacerbation until 10 min of treatment. Of note, following 10 min of Yoda1 exposure, ghosts were observed predominantly among old RBC (Fig. 5*B*; arrow).

A stepwise increase in sphericity of young RBC was observed within 5 min of Yoda1 treatment, which then plateaued (Fig. 5*C*), while middle and old RBC exhibited a partly reversal of the initial increase in sphericity following 10 min of Yoda1 exposure (both $P < 0.01$). Moreover, young RBC exhibited a stepwise decrease in area after 2, 5, and 10 min of Yoda1 treatment (Fig. 5*D*; all $P <$ 0.0001), while middle and old RBC presented with a steeper, less

gradual decrease. Old RBC had significantly elevated solidity at 0 min ($P < 0.0001$) over young and middle RBC. With Yoda1 exposure solidity increased within all subpopulations. Young and old RBC showed a reversal of the initially observed increase between 5 and 10 min of treatment ($P < 0.01$; Fig. 5*E*).

Given our initial observation of increased lysis susceptibility of old RBC in response to mechanical forces (Fig. 2) despite less pronounced Piezo1-dependent Ca^{2+} influx (Figs. 3 and 4), and the diminished capacity of old RBC to export Ca^{2+} (Fig. 3*C*) leading to acute and pronounced cell shrinkage (Fig. 5 *B* and *D* and *SI Appendix*, Fig. S3*C*), we aimed to directly characterize the RBC lysis process brought on by sustained Piezo1-induced entry of Ca^{2+}.

Calcium-Dependent Lysis of Old Erythrocytes is Preceded by Acute Cell Swelling. During prolonged exposure of RBC to 15 μmol L^{-1} Yoda1, accumulation of cytosolic Ca^{2+} was observed in concert with cell shrinkage (Fig. 5*D* and 6*C*). In the intermediate stage between high-density, low-volume spherocytes and ghost formation, however, continued accumulation of cytosolic Ca^{2+} eventually led some RBC within the old fraction to rapidly swell immediately prior to releasing cell contents, and fluorescence diminishing completely, indicating cell lysis (Movie S1). Further, Fluo-4 loaded RBC aspirated into the 2-μm micropipette tip (Fig. 4) held at a constant negative pressure exhibited a swelling and lysis response (Movie S2) identical to that observed in response to pharmacological Piezo1 activation (Movie S1).

Direct observation of cell lysis in response to prolonged exposure to Yoda1 confirmed that old RBC were significantly more sensitive to lysis due to Ca^{2+} influx when compared with young cells (Fig. 6*A*; $P < 0.0001$). Further, inhibition of PMCA with vanadate significantly prolonged time to lysis, irrespective of cell age (Fig. 6*B*; $P < 0.05$). When Ca^{2+}-induced lysis was brought on pharmacologically (i.e., *via* Yoda1), Fluo-4 fluorescence immediately increased in a nonlinear manner; however, when brought on mechanically (i.e., *via* micropipette aspiration), Fluo-4 fluorescence initially increased at a significantly slower rate (Fig. 6*C*; $P < 0.05$) before then following a nonlinear pattern similar to that observed with Yoda1 treatment, until lysis. Of note, cell swelling in RBC aspirated with the micropipette appeared to coincide with the sharp increase in Fluo-4 fluorescence noted at ~40% time to lysis (Fig. 6*C*)."

Discussion

Using a combination of pharmacological and mechanical stimulation of mechanosensitive cation channels on both bulk and single-cell levels, we provide evidence to support that some dense RBC are exceptionally susceptible to lysis following increased $[Ca^{2+}]_i$. It appears that susceptible RBC exhibit an impaired tolerance to increased $[Ca^{2+}]_i$, despite an apparent loss of Piezo1 in these same cells. It may be that this progressive loss of Piezo1 from RBC serves to balance the impaired Ca^{2+} tolerance. Once these cells are poised for removal from circulation, prolonged exposure to mechanical forces, such as during splenic transit, may promote an overload of $[Ca^{2+}]_i$, thus facilitating lysis and ghost formation. We hypothesize that sustained Piezo1 activation through prolonged exposure to mechanical forces (e.g., when old RBC adhere to the extracellular matrix of the spleen) rapidly drains cellular ATP by forcing substantial PMCA-activity to export cytosolic Ca^{2+}-under physiological conditions, the PMCA in RBC operates well-below maximal capacity (13). Resultant activation of the Gárdos channel causes K^+-efflux and induces cell shrinkage. Once metabolic capacity is insufficient to fuel the Na^+-K^+-ATPase, a rapid swelling event caused by influx of Na^+ results in acute lysis (Movies S1 and S2). While this hypothesis (Fig. 6*D*) is supported by the present data and compatible with recent advances (29, 30), in vivo experiments will be required for validation, although the fundamental physiological differences between typical animal models (e.g., mice (31)) and humans present challenges.

Hemolysis under low mechanical forces in the presence of extracellular Ca^{2+} has previously been observed (17), and it was reported that the remaining cells exhibited superior mechanical properties, when compared with an untreated blood sample (32). The present findings indicate that old RBC are particularly sensitive to lysis during prolonged mechanical force exposure only when Ca^{2+} is present, thus precipitating a surviving cell population that exhibits significantly improved cellular deformability ($P < 0.05$; Fig. 2 *B* and *D*) and increased MCV ($P < 0.05$; Fig. 2*G*). The Ca^{2+}-dependent removal observed here may thus be selective for RBC with unfavorable cell mechanics (e.g., old RBC), and we hypothesize that this may present a mechanism through which RBC are removed from circulation at the end of their lifespan.

Old RBC exhibit decreased Ca^{2+} extrusion rates (10, 33), likely related to decreased metabolic capacity and a lower basal ATP content (7, 8, 34). It is plausible that these metabolic deficits underpin our observation that old RBC accumulated $[Ca^{2+}]_i$ following stimulation with Yoda1, while RBC from other fractions did not (Fig. 3*C*). Old RBC also exhibited morphological changes at lower Yoda1 doses and exposure times when compared with the other fractions (Fig. 5 and *SI Appendix*, Fig. S2). Prevention of ATP depletion with pyruvate significantly depressed the Yoda1-dependent increase in $[Ca^{2+}]_i$ (*SI Appendix*, Fig. S6), indicating that the initial rate of Ca^{2+} export *via* PMCA is dependent upon the metabolic state of the cell. Moreover, although Piezo1 stimulation was standardized (i.e., Yoda1 concentration and suction pressure of the micropipette aspiration apparatus), RBC subpopulations exhibited distinct responses. It was unexpectedly observed that old RBC generally responded with a less pronounced influx of Ca^{2+} when stimulated with a range of Yoda1 concentrations (Fig. 3*B* and *SI Appendix*, Fig. S2) or directly exposed to mechanical force *via* micropipette aspiration (Fig. 4*D*), which may plausibly be due to age-dependent loss of membrane-bound Piezo1 (Fig. 3*D*). Given the absence of translational processes, it appears that RBC may actively release Piezo1 (e.g., through exocytosis); however, additional evidence is required to ascertain this hypothesis. Alternatively, it is also possible that existing Piezo1 channels decline in function with increasing cell age, or lose sensitivity to activation, resulting in overall diminished cellular Ca^{2+} transport capacity. We have previously shown that formation of disulfide bridges may directly interfere with Piezo1-dependent Ca^{2+} movement (23), and it is well known that oxidative modifications are increasingly prevalent in old RBC (35).

Despite the obvious clinical relevance of hemolysis, the precise mechanisms underlying this process are surprisingly poorly resolved [for a recent review, see ref. 36]. Our observations indicate that within the carefully isolated old RBC population (bottom 1% of RBC separated by density processing), only ~0.5% of cells are sensitive to lysis following acute Piezo1-induced uptake of Ca^{2+} and swelling (Fig. 6*A*), which equates to 0.005% of all RBC. This figure is remarkably consistent with the number of RBC that would be turned over during splenic transit in the average healthy adult male [0.003 to 0.008%; (37, 38)], considering typical splenic perfusion (39). Direct Ca^{2+}-dependent lysis of RBC has not been reported as a physiological mechanism (14), but as a commonly observed experimental by-product (40–42). Given the low number of highly susceptible RBC present in a typical blood sample, however, it is possible that these cells are lost during processing.

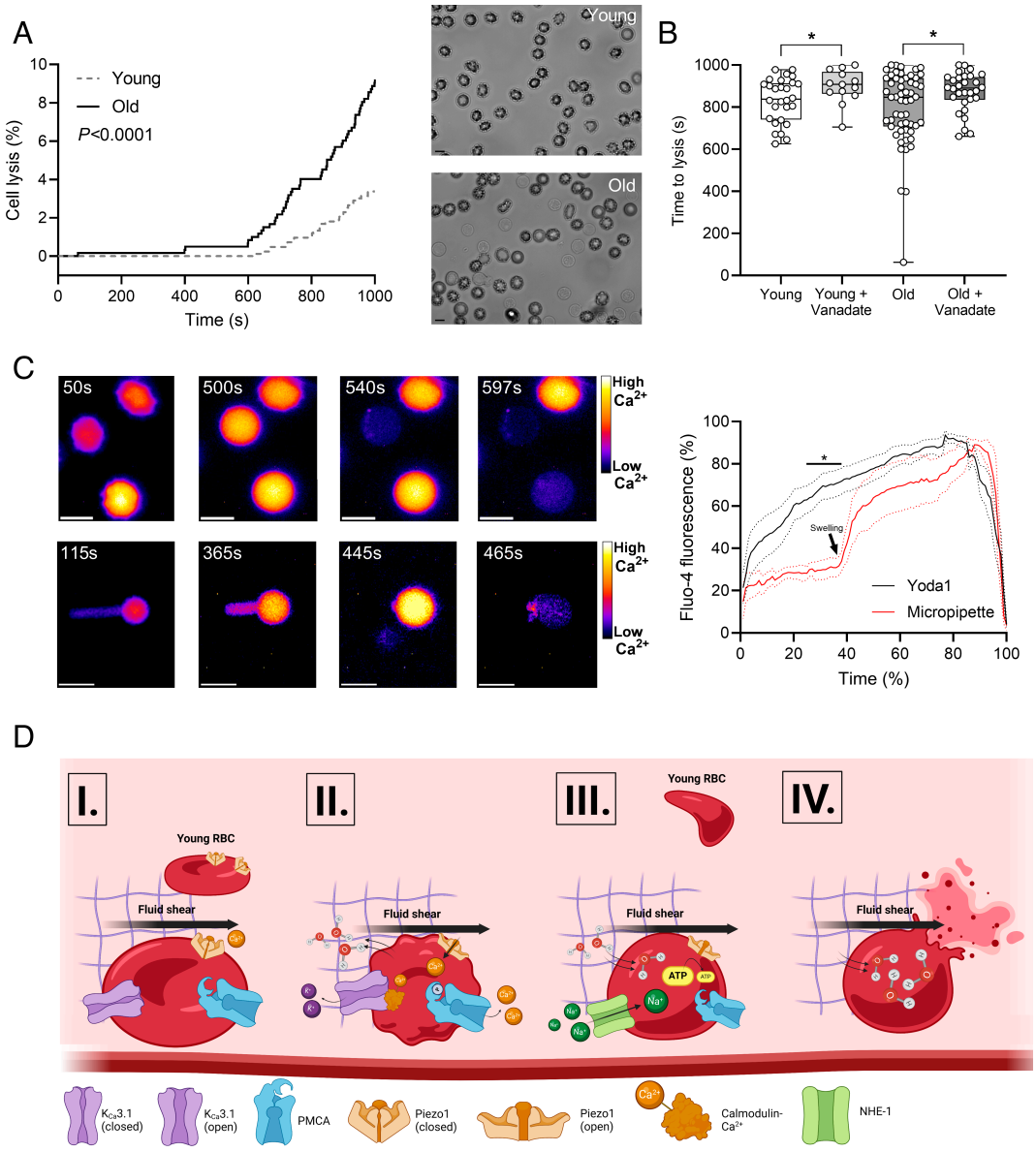

Fig. 6. Prolonged influx of calcium ions into old red blood cells (RBC) directly leads to cell lysis. Lysis of young and old RBC exposed to 15 μmol L^{-1} Yoda1 was monitored for up to 1,000 s, yielding lysis probability of each subpopulation, which was statistically compared using Kaplan–Meier analysis (*A*). *n* = 594 to 826 individual RBC from three distinct blood donors. Further, time to lysis of individual young and old RBC was measured and compared with lysis time of young and old RBC pretreated with the plasma membrane calcium pump (PMCA) inhibitor vanadate (*B*) using Mann–Whitney *U* tests. *n* = 13 to 55 individual RBC from three distinct blood donors. The fluorescent intensity of individual RBC isolated from the old cell fraction loaded with the calcium-sensitive fluorescent dye Fluo-4 was recorded until lysis during exposure to 15 μmol L^{-1} Yoda1 (*A*) or during aspiration into a 2-μm micropipette tip (*C*). *n* = 5 to 10 individual RBC from three distinct blood donors. Representative images of cells measured at different intervals of the lysis process are shown alongside traces of second-by-second mean fluorescent intensity obtained from all lysed RBC. Comparisons were performed using two-way ANOVA. $^{*}P < 0.05$. (Scale bars, 5 μm.) The hypothesized mechanism of RBC lysis is depicted in a schematic (*D*). Old RBC, which are highly adhesive due to expression of activated Lu/BCAM (purple mesh), bind to splenic laminin-a5 and remain attached (*I*). Younger nonadhesive RBC may temporarily adhere, however, will likely return to the bloodstream due to the fluid forces acting on these cells overpowering adhesion forces. Prolonged exposure to fluid shear forces as blood flows past the adhered old RBC activates mechanosensitive cation channels like Piezo1, prompting influx of calcium ions (Ca^{2+}). Sustained opening of Piezo1, and thus influx of Ca^{2+}, requires activation of PMCA at the expense of adenosine triphosphate (ATP) hydrolysis. Further, increased concentration of cytosolic Ca^{2+} activates the calcium-activated potassium channel $K_{Ca}3.1$. Activation of $K_{Ca}3.1$ results in efflux of potassium ions (K^{+}), which cause a change in osmotic pressure that drives water out of the cell, shrinking it (*II*). The RBC remains in this balanced state until ATP content is insufficient to facilitate removal of Ca^{2+} entering due to sustained Piezo1 opening. Once ATP is depleted, however, the sodium (Na^{+})-K^{+} pump is unable to maintain ionic gradients, and Na^{+} enters the cell, causing a reversal of the osmotic gradient. Entry of Na^{+} causes a rapid swelling of the old RBC due to reversal of osmotic gradients and uptake of water (*III*). Rapid, uncompensated uptake of water ultimately swells the cell until lysis occurs (*IV*), releasing cytosolic contents and thus leaving behind the RBC ghost.

Clinically, gain-of-function mutations of *PIEZO1* in humans have been linked with premature clearance of RBC and thus anemia (24, 25, 43). Further, pathologically increased $[Ca^{2+}]_i$ is considered a driving force behind accelerated in vivo aging of RBC in several hereditary anemias, thus facilitating premature clearance of still-intact, but fragile RBC (44). Indeed, both a lowered activation threshold and slowed inactivation of Piezo1 channels would exacerbate Ca^{2+} entry during each capillary transit. Excessively increased $[Ca^{2+}]_i$ accelerates RBC aging, thus producing a greater number of RBC that are susceptible to removal, while also directly promoting clearance of younger RBC, ultimately facilitating anemia.

Increased $[Ca^{2+}]_i$ has been reported to increase osmotic fragility of healthy RBC not due to altered cell volume, but through causing membrane area loss due to exovesicle production (40, 45). Sustained Piezo1 activation through Yoda1 exposure was observed

to cause membrane blebbing and production of exovesicles under the conditions studied here (*SI Appendix*, Fig. S7). In a recently proposed model of erythrophagocytosis (30), it was suggested that old RBC attach to the splenic architecture *via* adhesion molecules (46)–a process potentially facilitated by Gárdos channel activation – where subsequent exposure to prolonged mechanical force induces vesicle generation, and eventually ghost formation (29). Slow in vivo transit times of old RBC due to impaired cell deformability (47) and decreased capacity of these cells for shrinkage in response to mechanical forces may facilitate prolonged attachment. This prolonged mechanical stimulation of RBC in vivo is unusual in the context of normal circulatory transit, given the typically short and dynamic mechanical stresses experienced by cells during rapid microcirculatory passage (48), and may coincide with RBC removal.

We provide evidence to support some components of this hypothesis: We observed that old RBC are more susceptible to lysis under mechanical shear in the presence of Ca^{2+} than younger cells; old RBC present with impaired capacity to handle large increases in $[Ca^{2+}]_i$ induced by Piezo1 activation (i.e., mechanical force), which trigger the Gárdos effect; and significant production and release of extracellular vesicles occurs in response to sustained Piezo1 activation (*SI Appendix*, Fig. S7). Interestingly, while Yoda1 exposure initially resulted in RBC shrinkage, immediately preceding lysis, a rapid swelling response was observed (9) (Movies S1 and S2). We pose the hypothesis that the sustained Ca^{2+} influx *via* Piezo1 caused by prolonged mechanical force exposure, which only occurs when RBC are in a slow-transit and high-shear region like the splenic sinusoids, rapidly drains cellular energy (i.e., ATP). Once ATP is insufficient to fuel active transport, uncompensated inward leakage of Na^+ facilitates entry of water and cell swelling until membrane rupture (Fig. 6*D*); this is supported by the observation that swelling coincides with a strong acceleration in Ca^{2+} uptake (Fig. 6*C*). The kinetics of this process would be in the order of minutes, which is likely more reflective of residence times than previous models that proposed proteolytic digestion of the membrane secondary to ion leakage (30). Subsequently, the resident splenic macrophage population is equipped to recycle the released hemoglobin locally, thus preventing excessive levels of free hemoglobin into the plasma (49).

Recent advances support that transient receptor potential vanilloid type 2 (TRPV2), another cation channel that may be mechanosensitive, is also expressed in mammalian RBC (50, 51). Whether channels of the TRP family are inherently mechanosensitive (52, 53) or rather act downstream of mechanosensors like Piezo1 (54) remains to be determined, although recent evidence supports the latter [reviewed in (55)]. Further, while pharmacological stimulation of TRPV2 was shown to facilitate Ca^{2+} influx into RBC (51), evidence of TRPV2-dependent mechanically induced Ca^{2+} influx is yet to be provided. Given that the inhibitory peptide GsMTx4 is not specific for Piezo1, but rather inhibits most known mechanosensitive ion channels (56), it is possible that cation channels other than Piezo1 are involved in the mechanical force-dependent Ca^{2+}-induced lysis mechanism proposed here (Fig. 6*D*). Future studies employing genetic models should dispel residual doubts about the molecular identity of mechanosensitive channels involved in RBC responses.

Methods

Blood Sample Collection. Participants were healthy, male volunteers, who had not provided a large-volume blood donation (i.e., 450 mL) within 3 mo, and were not taking medication. Written and informed consent was obtained, and blood samples were collected from the antecubital region into tubes containing ethylenediaminetetraacetic acid (1.8 mg mL^{-1}). All experimental procedures were reviewed and approved by the Human Research Ethics Committee of Griffith University (2020/093, Gold Coast, Australia) and align with the Declaration of Helsinki. All experimental procedures were completed within 6 h of blood collection.

Sample Processing and Density Separation of Erythrocyte Subpopulations. RBC were isolated by centrifugation at 1,500×*g* for 10 min and then washed three times with an isotonic phosphate-buffered saline (PBS) solution supplemented with bovine serum albumin (BSA; 0.8 g mL^{-1}) and 5 mmol L^{-1} glucose (GASP; pH = 7.4 ± 0.05, 290 ± 5 mOsmol·kg^{-1}). RBC were resuspended in a serum albumin-HEPES buffer (SAH; pH = 7.1 ± 0.05; 26 g L^{-1} albumin) and layered upon a gradient of Percoll-SAH mixtures of distinct densities (1.063, 1.066, 1.069, and 1.071 g mL^{-1}). Separation was achieved by centrifugation at 3,260×*g* for 40 min at room temperature (57). Three distinct RBC subpopulations were isolated based on their densities (Fig. 1*A*; "light," "middle" and "dense" fractions; in the following referred to as "young," "middle" and "old" RBC), washed with GASP-buffer, and then used in subsequent analyses.

Hematological Analysis and Glycated Hemoglobin Concentration. Hematological parameters of isolated RBC subpopulations were analyzed using an automated cell counter (DxH 500, Beckman Coulter, Brea). The same device was also used to monitor mean cell volume (MCV) following mechanical force exposure.

Glycated hemoglobin (HbA1c) was measured using the Human Hemoglobin A1c ELISA Kit (ab289836; Abcam, Melbourne, VIC, Australia) according to the manufacturer's instructions and normalized to total hemoglobin concentration.

Erythrocyte Deformability and Bulk Mechanical Stress Application. A rotational Couette-type ektacytometer (LORCA, MaxSis, Mechatronics Instruments B.V., Zwaag, The Netherlands) was used to quantify cellular deformability (58) and expose RBC to well-controlled shear stress (17, 59, 60) (i.e., 10 Pa for 300 s) at 37 ± 0.2 °C. Isolated RBC were resuspended in a viscous polyvinylpyrrolidone solution (PVP 360 kDa dissolved in PBS; pH = 7.4 ± 0.5, 290 ± 5 mOsmol·kg^{-1}, viscosity = 30.0 ± 0.5 mPa s) at a hematocrit of 0.005 L L^{-1}. For some experiments, the PVP solution also contained calcium at a plasma-equivalent concentration (i.e., 2 mmol L^{-1} $CaCl_2$).

Free Hemoglobin Concentration. Immediately following shear stress exposure, RBC-PVP suspensions were collected from the cup of the shearing device. The supernatant was collected following centrifugation at 3,000×*g* for 10 min and diluted in 0.01% Na_2CO_3 solution at a 1:1 ratio. Free hemoglobin concentration was measured using the Harboe method (61). A positive control was prepared by lysing 0.005 L L^{-1} RBC in distilled water, and hemolysis values were calculated relative to this positive control to facilitate interpretation.

Live Cell Calcium Imaging. Changes in $[Ca^{2+}]_i$ were monitored using Fluo-4 (62). Isolated RBC were washed thrice with Tyrode's buffer containing 10 mmol L^{-1} HEPES and glucose, respectively, and then loaded with 5 μmol L^{-1} Fluo-4 AM (23). For some experiments, 5 mmol L^{-1} sodium pyruvate was included in the Fluo-4 loading medium to prevent depletion of cellular ATP (*SI Appendix*, Fig. S6). For other experiments, Fluo-4 loaded RBC were incubated with 1 mmol L^{-1} of the PMCA-inhibitor sodium orthovanadate for 30 min at room temperature. Loaded RBC were transferred onto coverslips and incubated at room temperature for 15 min to allow for cell sedimentation and de-esterification of the dye. The fluorescent intensity was recorded during exposure to an argon laser (excitation λ = 488 nm/emission λ = 508 nm). RBC were then incubated with 15 μmol L^{-1} of the Piezo1-specific activator Yoda1 for 10 min. Immediately following Yoda1 exposure, images of one region of interest were captured with a frequency of 0.067 Hz for up to 10 min.

Micropipette Aspiration. The micropipette aspiration rig was custom developed (63) and is described in more detail in *SI Appendix*, Supplementary Materials. Briefly, elongated glass pipettes with inner diameters comparable to those of small capillaries (2 to 3 μm) were manufactured from borosilicate capillary tubes. Fluo-4-loaded RBC were aspirated through the narrow pipette tip, forcing elongation. Changes in fluorescent intensity, reflective of $[Ca^{2+}]_i$, and cell behavior during deformation were visualized using an inverted microscope (IX73, Olympus Corporation, Japan) coupled to a high-speed CMOS camera (optiMOS sCMOS, QImaging, Surrey, SA, Australia).

Immunofluorescent Detection of Piezo1. Following density fractionation of young, middle, and old RBC subpopulations, autologous plasma was added to each RBC subfraction to produce 0.4 L L^{-1} cell suspensions. RBC were fixed in 4% PFA for 20 min, and blood smears were produced as previously described (64, 65). The immunofluorescent detection protocol was as described in (65). Primary antibody was directed against the Piezo1 extracellular domain (rabbit polyclonal; 1:500; Cat no.: 15939-1-AP, Proteintech Group Inc., Rosemont) and detected using goat anti-rabbit secondary antibody (1:400 dilution; Alexa Fluor 568, Thermo Fisher, Scoresby, Australia). Imaging of fluorescently labeled Piezo1 was performed using the inverted microscope at 600-fold magnification (excitation $\lambda = 594$ nm/emission $\lambda = 614$ nm).

Data analysis. Raw EI-SS curves were parameterized using a nonlinear version of the Lineweaver–Burk equation (66), adapted to most accurately represent mechanical properties of RBC with diverse cell volumes (17). The fluorescent intensity of immunolabeled or Fluo-4 loaded RBC was determined using open-source software [FIJI version 1.53c (67), NIH, Bethesda, MD]. A minimum of 150 individual RBC were analyzed for Fluo-4 mean fluorescent intensity, a minimum 100 individual cells for the test areas of immuno-tagged Piezo1, and a minimum of 50 individual cells for the respective control areas not containing Piezo1-specific antibodies. Immunofluorescence data were analyzed using an automated thresholding macro as previously described (65).

Brightfield microscopy data were analyzed using "RedTell" (68), which is described in more detail in *SI Appendix*, Supplementary materials. Briefly, a pretrained Mask R-CNN-based artificial neural network generates segmentation masks of individual cells for a given image. Then, following optimization (filtering) of segmentation results, morphological cell features are extracted from the obtained masks (*SI Appendix*, Fig. S1). Cell features presented here were chosen based on biological relevance; Yoda1 induces cell shrinkage due to the Gárdos effect, which would affect cell area and sphericity. Solidity was previously shown to be relevant during the discocyte–echinocyte transformation (68).

Statistical analysis. Results are presented as means ± SD, unless otherwise stated. Distribution of data was tested for normality using the Shapiro–Wilk test. Differences in EI-shear stress curves and Fluo-4 fluorescent intensities over time were analyzed using two-way ANOVAs. Depending on normality of distribution, differences between group means were determined using either a conventional one-way ANOVA with Dunnett's post hoc test for multiple comparisons or a Friedman test with Dunn's correction. Where means of two groups were compared, two-tailed *t* tests or Mann–Whitney *U* tests were employed, depending on data distribution. Statistically significant differences between the lysis likelihood of young and old cell populations were computed using Kaplan–Meier survival analysis. Statistical analyses and curve fitting were performed using commercial software (Prism, GraphPad Software Inc., Release 9.2.0, La Jolla, CA). Differences were considered significant at an alpha level of 0.05.

Data, Materials, and Software Availability. All study data are included in the article and/or Supporting Information.

ACKNOWLEDGMENTS. LK was supported through the Griffith University Postgraduate Fellowship scheme. APM was supported by the Australian Research Council (DP230100556; DE240100236). MB was supported by the Helmholtz Association under the joint research school "Munich School for Data Science–MUDS." MJS was supported by the Australian Research Council (DP230100556) and Medical Research Future Fund (RFRHPI000241). Figs. 4 and 6 were produced using BioRender. CM received funding from the European Research Council under the European Union's Horizon 2020 Research and Innovation Program (Grant agreement 866411) and support from the Hightech Agenda Bayern.

Author affiliations: [a]Biorheology Research Laboratory, Griffith University, QLD 4215, Australia; [b]Institute of Computational Biology, Computational Health Center, Helmholtz Munich, Munich 85764, Germany; [c]Department of Biology, Ludwig-Maximilians University Munich, Munich 80539, Germany; [d]Data and Analytics, Pharmaceutical Research and Early Development, Roche Innovation Center Munich, Penzberg 82377, Germany; [e]Institute of AI for Health, Helmholtz Zentrum München–German Research Center for Environmental Health, Neuherberg 85764, Germany; [f]Computer Aided Medical Procedures, Technical University of Munich 85748, Germany; and [g]School of Pharmacy and Medical Sciences, Griffith University Gold Coast, QLD 4215, Australia

Author contributions: L.K., A.P.M., C.M., J.N.P., and M.J.S. designed research; L.K. and A.P.M. performed research; L.K., A.P.M., M.B., A.S., and M.J.S. contributed new reagents/analytic tools; L.K., M.B., A.S., C.M., J.N.P., and M.J.S. analyzed data; and L.K., A.P.M., M.B., A.S., C.M., J.N.P., and M.J.S. wrote the paper.

1. O. K. Baskurt, H. J. Meiselman, Blood rheology and hemodynamics. *Semin. Thromb. Hemost.* **29**, 435–450 (2003).
2. S. Chien, Red cell deformability and its relevance to blood flow. *Annu. Rev. Physiol.* **49**, 177–192 (1987).
3. F. H. Bosch *et al.*, Determinants of red blood cell deformability in relation to cell age. *Eur. J. Haematol.* **52**, 35–41 (1994).
4. I. Safeukui *et al.*, Sensing of red blood cells with decreased membrane deformability by the human spleen. *Blood Adv.* **2**, 2581–2587 (2018).
5. Y. Gottlieb *et al.*, Physiologically aged red blood cells undergo erythrophagocytosis in vivo but not in vitro. *Haematologica* **97**, 994–1002 (2012).
6. R. van Wijk, W. W. van Solinge, The energy-less red blood cell is lost: Erythrocyte enzyme abnormalities of glycolysis. *Blood* **106**, 4034–4042 (2005).
7. M. Magnani *et al.*, The age-dependent metabolic decline of the red blood cell. *Mech. Ageing Dev.* **22**, 295–308 (1983).
8. R. E. Bernstein, Alterations in metabolic energetics and cation transport during aging of red cells. *J. Clin. Invest.* **38**, 1572–1586 (1959).
9. C. H. Joiner, P. K. Lauf, Ouabain binding and potassium transport in young and old populations of human red cells. *Membr. Biochem.* **1**, 187–202 (1978).
10. V. L. Lew *et al.*, Effects of age-dependent membrane transport changes on the homeostasis of senescent human red blood cells. *Blood* **110**, 1334–1342 (2007).
11. A. Bogdanova, A. Makhro, J. Wang, P. Lipp, L. Kaestner, Calcium in red blood cells-a perilous balance. *Int. J. Mol. Sci.* **14**, 9848–9872 (2013).
12. V. L. Lew, R. Y. Tsien, C. Miner, R. M. Bookchin, Physiological [Ca2+]i level and pump-leak turnover in intact red cells measured using an incorporated Ca chelator *Nature* **298**, 478–481 (1982).
13. G. Dagher, V. L. Lew, Maximal calcium extrusion capacity and stoichiometry of the human red cell calcium pump. *J. Physiol.* **407**, 569–586 (1988).
14. V. L. Lew *et al.*, Distribution of plasma membrane Ca2+ pump activity in normal human red blood cells. *Blood* **102**, 4206–4213 (2003).
15. F. H. Bosch *et al.*, Characteristics of red blood cell populations fractionated with a combination of counterflow centrifugation and Percoll separation. *Blood* **79**, 254–260 (1992).
16. S. Rogers, V. L. Lew, PIEZO1 and the mechanism of the long circulatory longevity of human red blood cells. *PLoS Comput. Biol.* **17**, e1008496 (2021).
17. L. Kuck, J. N. Peart, M. J. Simmonds, Calcium dynamically alters erythrocyte mechanical response to shear. *Biochim. Biophys. Acta Mol. Cell Res.* **1867**, 118802 (2020).
18. G. Gardos, The function of calcium in the potassium permeability of human erythrocytes. *Biochim. Biophys. Acta* **30**, 653–654 (1958).
19. T. J. Simons, Calcium-dependent potassium exchange in human red cell ghosts. *J. Physiol.* **256**, 227–244 (1976).
20. A. D. Maher, P. W. Kuchel, The Gardos channel: A review of the Ca2+-activated K+ channel in human erythrocytes *Int. J. Biochem. Cell Biol.* **35**, 1182–1197 (2003).
21. J. G. Danielczok *et al.*, Red blood cell passage of small capillaries is associated with transient Ca(2+)-mediated adaptations. *Front. Physiol.* **8**, 979 (2017).
22. S. M. Cahalan *et al.*, Piezo1 links mechanical forces to red blood cell volume. *Elife* **4**, e07370 (2015).
23. L. Kuck, J. N. Peart, M. J. Simmonds, Piezo1 regulates shear-dependent nitric oxide production in human erythrocytes. *Am. J. Physiol. Heart Circ. Physiol.* **323**, H24–H37 (2022).
24. J. Albuisson *et al.*, Dehydrated hereditary stomatocytosis linked to gain-of-function mutations in mechanically activated PIEZO1 ion channels. *Nat. Commun.* **4**, 1884 (2013).
25. E. Glogowska *et al.*, Novel mechanisms of PIEZO1 dysfunction in hereditary xerocytosis. *Blood* **130**, 1845–1856 (2017).
26. S. Rogers, V. L. Lew, Up-down biphasic volume response of human red blood cells to PIEZO1 activation during capillary transits. *PLoS Comput. Biol.* **17**, e1008706 (2021).
27. L. Kuck, J. N. Peart, M. J. Simmonds, Active modulation of human erythrocyte mechanics. *Am. J. Physiol. Cell Physiol.* **319**, C250–C257 (2020).
28. K. J. Richardson, L. Kuck, M. J. Simmonds, Beyond oxygen transport: Active role of erythrocytes in the regulation of blood flow. *Am. J. Physiol. Heart Circ. Physiol.* **319**, H866–H876 (2020), 10.1152/ajpheart.00441.2020.
29. T. R. L. Klei *et al.*, Hemolysis in the spleen drives erythrocyte turnover. *Blood* **136**, 1579–1589 (2020).
30. R. J. Asaro, P. Cabrales, The RBC's road to ghost and removal: Splenic clearance. *Blood Adv.* **5**, 4422–4425 (2021).
31. B. S. Steiniger, Human spleen microanatomy: Why mice do not suffice. *Immunology* **145**, 334–346 (2015).
32. D. Sakota *et al.*, Mechanical damage of red blood cells by rotary blood pumps: Selective destruction of aged red blood cells and subhemolytic trauma. *Artif Organs* **32**, 785–791 (2008).
33. P. J. Romero, E. A. Romero, Differences in Ca2+ pumping activity between sub-populations of human red cells *Cell Calcium* **21**, 353–358 (1997).
34. H. J. Schatzmann, ATP-dependent Ca++-extrusion from human red cells *Experientia* **22**, 364–365 (1966).
35. J. G. Mohanty, E. Nagababu, J. M. Rifkind, Red blood cell oxidative stress impairs oxygen delivery and induces red blood cell aging. *Front. Physiol.* **5**, 84 (2014).
36. S. Waldvogel Abramowski, Hemolysis: Mechanism and clinico-biological consequences. *Transfus Clin. Biol.* **28**, 364–366 (2021).
37. J. M. Higgins, Red blood cell population dynamics. *Clin Lab Med* **35**, 43–57 (2015).
38. P. Thiagarajan, C. J. Parker, J. T. Prchal, How Do Red Blood Cells Die? *Front. Physiol.* **12**, 655393 (2021).
39. A. Oguro *et al.*, Quantification of human splenic blood flow (quantitative measurement of splenic blood flow with H2(15)O and a dynamic state method: 1). *Ann. Nucl. Med.* **7**, 245–250 (1993).
40. A. Cueff *et al.*, Effects of elevated intracellular calcium on the osmotic fragility of human red blood cells. *Cell Calcium* **47**, 29–36 (2010).

41. V. L. Lew, J. Garcia-Sancho, Measurement and control of intracellular calcium in intact red cells. *Methods Enzymol.* **173**, 100–112 (1989).
42. S. L. Thomas, Intravascular hemolysis: The sacrifice of few. *Blood* **124**, 2011–2012 (2014).
43. S. Martin-Almedina, S. Mansour, P. Ostergaard, Human phenotypes caused by PIEZO1 mutations; one gene, two overlapping phenotypes? *J. Physiol.* **596**, 985–992 (2018).
44. L. Hertz *et al.*, Is increased intracellular calcium in red blood cells a common component in the molecular mechanism causing anemia?. *Front. Physiol.* **8**, 673 (2017).
45. K. Thangaraju, S. N. Neerukonda, U. Katneni, P. W. Buehler, Extracellular vesicles from red blood cells and their evolving roles in health, coagulopathy and therapy. *Int. J. Mol. Sci.* **22** (2020).
46. T. R. L. Klei *et al.*, The Gardos effect drives erythrocyte senescence and leads to Lu/BCAM and CD44 adhesion molecule activation. *Blood Adv.* **4**, 6218–6229 (2020).
47. H. Li, Z. L. Liu, L. Lu, P. Buffet, G. E. Karniadakis, How the spleen reshapes and retains young and old red blood cells: A computational investigation. *PLoS Comput. Biol.* **17**, e1009516 (2021).
48. A. G. Koutsiaris, S. V. Tachmitzi, N. Batis, Wall shear stress quantification in the human conjunctival pre-capillary arterioles in vivo. *Microvasc. Res.* **85**, 34–39 (2013).
49. T. Ganz, Macrophages and Iron metabolism. *Myeloid Cells in Health and Disease: A Synthesis*, 803–812 (2017).
50. A. Belkacemi *et al.*, The TRPV2 channel mediates Ca2+ influx and the Delta9-THC-dependent decrease in osmotic fragility in red blood cells. *Haematologica* **106**, 2246–2250 (2021).
51. D. Flormann *et al.*, Transient receptor potential channel vanilloid type 2 in red cells of cannabis consumer. *Am. J. Hematol.* **97**, E180–E183 (2022).
52. Y. A. Nikolaev *et al.*, Mammalian TRP ion channels are insensitive to membrane stretch. *J. Cell Sci.* **132**, jcs238360 (2019).
53. K. Shibasaki, Physiological significance of TRPV2 as a mechanosensor, thermosensor and lipid sensor. *J. Physiol. Sci.* **66**, 359–365 (2016).
54. S. M. Swain, R. A. Liddle, Piezo1 acts upstream of TRPV4 to induce pathological changes in endothelial cells due to shear stress. *J. Biol. Chem.* **296**, 100171 (2021).
55. C. D. Cox, K. Poole, B. Martinac, Re-evaluating TRP channel mechanosensitivity. *Trends Biochem. Sci.* **49**, 693–702 (2024), 10.1016/j.tibs.2024.05.004.
56. R. Gnanasambandam *et al.*, GsMTx4: Mechanism of Inhibiting Mechanosensitive Ion Channels. *Biophys. J.* **112**, 31–45 (2017).
57. D. A. Bizjak, C. Brinkmann, W. Bloch, M. Grau, Increase in Red Blood Cell-Nitric Oxide Synthase Dependent Nitric Oxide Production during Red Blood Cell Aging in Health and Disease: A Study on Age Dependent Changes of Rheologic and Enzymatic Properties in Red Blood Cells. *PloS one* **10**, e0125206 (2015).
58. M. R. Hardeman, J. G. Dobbe, C. Ince, The Laser-assisted Optical Rotational Cell Analyzer (LORCA) as red blood cell aggregometer. *Clin. Hemorheol. Microcirc.* **25**, 1–11 (2001).
59. L. Kuck, M. Grau, M. J. Simmonds, Recovery time course of erythrocyte deformability following exposure to shear is dependent upon conditioning shear stress. *Biorheology* **54**, 141–152 (2018).
60. L. Kuck, M. Grau, W. Bloch, M. J. Simmonds, Shear stress ameliorates superoxide impairment to erythrocyte deformability with concurrent nitric oxide synthase activation. *Front. Physiol.* **10**, 36 (2019).
61. M. Harboe, A method for determination of hemoglobin in plasma by near-ultraviolet spectrophotometry. *Scand J. Clin. Lab Invest.* **11**, 66–70 (1959).
62. L. Kaestner, W. Tabellion, E. Weiss, I. Bernhardt, P. Lipp, Calcium imaging of individual erythrocytes: Problems and approaches. *Cell Calcium* **39**, 13–19 (2006).
63. A. P. McNamee, G. D. Tansley, M. J. Simmonds, Sublethal mechanical shear stress increases the elastic shear modulus of red blood cells but does not change capillary transit velocity. *Microcirculation* **27**, e12652 (2020).
64. F. Suhr *et al.*, Moderate exercise promotes human RBC-NOS activity, NO production and deformability through Akt kinase pathway. *PLoS One* **7**, e45982 (2012).
65. M. Grau, L. Kuck, Immunostaining-based detection of dynamic alterations in red blood cell proteins. *J. Vis. Exp.* **193**, e64843 (2023), 10.3791/64843.
66. O. K. Baskurt *et al.*, Parameterization of red blood cell elongation index–shear stress curves obtained by ektacytometry. *Scand J. Clin. Lab Invest.* **69**, 777–788 (2009).
67. J. Schindelin *et al.*, Fiji: An open-source platform for biological-image analysis. *Nat. Methods* **9**, 676–682 (2012).
68. A. Sadafi *et al.*, RedTell: An AI tool for interpretable analysis of red blood cell morphology. *Front. Physiol.* **14**, 1058720 (2023).